A Novel Small Molecule Targets Androgen Receptor and Its Splice Variants in Castration-Resistant Prostate Cancer

Zhenyu Yang[1,2,3], Dan Wang[3], James K. Johnson[4], Laura E. Pascal[3], Keita Takubo[4], Raghunandan Avula[5], Anish Bhaswanth Chakka[5], Jianhua Zhou[3], Wei Chen[3], Mingming Zhong[3], Qiong Song[3,6], Hui Ding[3], Zeyu Wu[3], Uma R. Chandran[5], Taber S. Maskrey[4], Joel B. Nelson[3,7], Peter Wipf[4,7], and Zhou Wang[3,7,8]

ABSTRACT

Reactivation of androgen receptor (AR) appears to be the major mechanism driving the resistance of castration-resistant prostate cancer (CRPC) to second-generation antiandrogens and involves AR overexpression, AR mutation, and/or expression of AR splice variants lacking ligand-binding domain. There is a need for novel small molecules targeting AR, particularly those also targeting AR splice variants such as ARv7. A high-throughput/high-content screen was previously reported that led to the discovery of a novel lead compound, 2-(((3,5-dimethylisoxazol-4-yl)methyl)thio)-1-(4-(2,3-dimethylphenyl)piperazin-1-yl)ethan-1-one (IMTPPE), capable of inhibiting nuclear AR level and activity in CRPC cells, including those resistant to enzalutamide. A novel analogue of IMTPPE, JJ-450, has been investigated with evidence for its direct and specific inhibition of AR transcriptional activity via a pulldown assay and RNA-sequencing analysis, PSA-based luciferase, qPCR, and chromatin immunoprecipitation assays, and xenograft tumor model 22Rv1. JJ-450 blocks AR recruitment to androgen-responsive elements and suppresses AR target gene expression. JJ-450 also inhibits ARv7 transcriptional activity and its target gene expression. Importantly, JJ-450 suppresses the growth of CRPC tumor xenografts, including ARv7-expressing 22Rv1. Collectively, these findings suggest JJ-450 represents a new class of AR antagonists with therapeutic potential for CRPC, including those resistant to enzalutamide.

Introduction

Prostate cancer is the most commonly diagnosed noncutaneous malignancy and the second leading cause of cancer death among men in the United States (1). Androgen deprivation therapy is the standard and initially effective treatment for patients with metastatic prostate cancer, but most will eventually develop castration-resistant prostate cancer (CRPC), defined as androgen receptor (AR) activation despite castrate levels of androgen (2–6). Second-generation AR inhibitors were developed or are under development for the treatment of CRPC, including the selective androgen biosynthesis inhibitor abiraterone (7) and AR antagonists, such as enzalutamide (MDV3100; ref. 8), apalutamide (ARN-509; refs. 9, 10), and darolutamide (ODM-201; ref. 11). These inhibitors can prolong the survival of patients with CRPC for several months with most developing resistance (12–14).

Resistance to second-generation AR inhibitors is largely the result of AR reactivation through multiple mechanisms, including upregulation of AR and CYP17 expression, emergence of AR point mutations, constitutively active AR splice variants, and increased intratumoral androgen synthesis (15–18). As such, AR remains an important therapeutic target for CRPC resistant to second-generation AR inhibitors, with the need for novel anti-AR agents.

The current group of FDA-approved AR-targeting agents acts either directly or indirectly through the AR ligand-binding domain (LBD), which increases the likelihood of cross-resistance to these therapeutic agents. To overcome resistance to enzalutamide and/or abiraterone, new anti-AR therapeutics targeting different domain(s) of AR, such as the N-terminal domain (NTD) or DNA-binding domain (DBD), is a reasonable strategy. Several small molecules, including EPI-001 for targeting NTD (19), VPC-14228 and VPC-14449 for targeting DBD (20), and SARDs for targeting both DBD and LBD (21), are being developed for CRPC treatment. The identification and development of small molecules targeting AR through other mechanisms will enhance the possibility of clinically useful AR inhibitors.

Recently, a high-throughput/high-content screening campaign of 219,055 small molecules was reported, identifying a novel AR antagonist, 2-(((3,5-dimethylisoxazol-4-yl)methyl)thio)-1-(4-(2,3-dimethylphenyl)piperazin-1-yl)ethan-1-one (IMTPPE), based on its ability to inhibit nuclear AR levels in CRPC cells (22). IMTPPE blocked the expression of AR-target genes, inhibited the proliferation of AR-positive cancer cells, and suppressed the growth of xenograft tumors expressing AR variants. IMTPPE inhibition of AR did not require the LBD, as this compound inhibited the activity of a mutant AR lacking the LBD (23). Because the structure of IMTPPE

[1]Department of Urology, Sun Yat-sen University Cancer Center, Guangzhou, Guangdong, P.R. China. [2]The Third Xiangya Hospital, Central South University, Changsha, Hunan, P.R. China. [3]Department of Urology, University of Pittsburgh School of Medicine, Pittsburgh, Pennsylvania. [4]Department of Chemistry, University of Pittsburgh, Pittsburgh, Pennsylvania. [5]Department of Biomedical Informatics, University of Pittsburgh, Pittsburgh, Pennsylvania. [6]Key Laboratory of Longevity and Aging-Related Diseases, Guangxi Medical University, Ministry of Education, Nanning, Guangxi, P.R. China. [7]UPMC Hillman Cancer Center, University of Pittsburgh School of Medicine, Pittsburgh, Pennsylvania. [8]Department of Pharmacology and Chemical Biology, University of Pittsburgh School of Medicine, Pittsburgh, Pennsylvania.

Note: Supplementary data for this article are available at Molecular Cancer Therapeutics Online (http://mct.aacrjournals.org/).

Corresponding Authors: Zhou Wang, University of Pittsburgh School of Medicine, 5200 Centre Avenue, Suite G40, Pittsburgh, PA 15232. Phone: 412-623-3903; Fax: 412-623-3904; E-mail: wangz2@upmc.edu; and Peter Wipf, 758 CHVRN Chevron Science Center, 219 Parkman Avenue, Pittsburgh, PA 15260. E-mail: pwipf@pitt.edu

Mol Cancer Ther 2020;19:75–88

doi: 10.1158/1535-7163.MCT-19-0489

is distinct from known antiandrogens and it inhibited AR lacking the LBD, IMTPPE can be considered as a new AR antagonist and may provide an opportunity to inhibit growth in CRPC resistant to second-generation AR inhibitors.

Here, the mechanism of IMTPPE's inhibition of AR is further investigated with characterization of JJ-450, an IMTPPE scaffold variant with improved potency and physicochemical properties. JJ-450 (originally designated Compound 27) is a racemic mixture of two stereoisomers, (−)-JJ-450 and (+)-JJ-450, with (−)-JJ-450 being approximately 9-fold more potent than (+)-JJ-450 in the luciferase PSA-reporter assay (24). In this study, the binding of IMTPPE to AR was tested, JJ-450's inhibition of AR and ARv7 transcriptional activities was assessed, JJ-450's specificity of AR inhibition was compared with enzalutamide, and the efficacy of JJ-450 in prostate xenograft tumors was determined, including those resistant to enzalutamide.

Materials and Methods

Cell lines and key resources

LNCaP, 22Rv1, VCaP, and PC3 prostate cancer cell lines were obtained from the American Type Culture Collection. C4-2 (25), LAPC4 (26), CWR-R1 (27), and GFP-ARv7:PC3 (28) cell lines were kindly provided by Dr. Leland W.K. Chung (Cedars-Sinai Medical Center), Dr. Robert Reiter (University of California, California, LA), Dr. Christopher W. Gregory (University of North Carolina, Chapel Hill, NC), and Dr. Michael Mancini (Baylor College of Medicine, Huston, TX), respectively. C4-2-PSA-rl (24) and PC3-AR (29) stable cell lines were generated internally. All cells were maintained at 37°C in a 5% CO_2 incubator, grown in complete medium supplemented with 10% FBS (Atlanta Biologicals), L-glutamine (2 mmol/L), penicillin (100 U/mL), and streptomycin (100 μg/mL). LNCaP, 22Rv1, PC3, C4-2, and CWR-R1 cells were grown in complete RPMI medium (Corning). VCaP cells were maintained in complete DMEM medium (Lonza). LAPC4 cells were grown in IMDM (HyClone) supplemented with 1 nmol/L R1881 (PerkinElmer). PC3-AR cells were maintained in complete RPMI medium supplemented with 500 μg/mL G418. GFP-ARv7:PC3 cells were grown in complete DMEM/F12 (Corning) supplemented with 500 μg/mL G418. C4-2-PSA-rl cells were cultured in RPMI supplemented with 10 μg/mL puromycin and 500 μg/mL G418. The genetic identity of 22Rv1, C4-2, VCaP, and LNCaP cell lines was authenticated in 2016 using DNA fingerprinting by examining microsatellite loci in a multiplex PCR (AmpFlSTR Identifiler PCR Amplification Kit, Applied Biosystems) by the University of Pittsburgh Cell Culture and Cytogenetics Facility. Cell lines were confirmed as *Mycoplasma* free by PCR testing on a monthly basis, and all key experiments were performed using cell lines between passages 4 and 28. Key resources are listed in Supplementary Table S1.

Xenograft mouse models

Male Crl:SHO-*Prkdc*^{scid}*Hr*^{hr} mice ages 6 to 8 weeks old were obtained from Charles River Laboratory. Animal care and use were reviewed and approved by the Institutional Animal Care and Use Committee of the University of Pittsburgh (protocol #17019973). LNCaP (3×10^6 cells), C4-2 (3×10^6 cells), VCaP (2.7×10^6 cells), or 22Rv1 (1×10^6 cells) suspended in 150 μL medium were gently mixed with 150 μL of Matrigel and then inoculated subcutaneously in the right-flank region of male Crl:SHO-*Prkdc*^{scid}*Hr*^{hr} mice. Tumor volume was calculated using the modified ellipsoid formula: length × width^2 × 0.52 (30). For the short-term study in the LNCaP model (**Fig. 6A–E**), castration was performed when tumor volume reached approximately 200 mm^3. When tumor volume reached approximately 300 mm^3, mice were randomized and treated with enzalutamide (10 mg/kg body weight i.p.) or JJ-450 (25 mg/kg body weight i.p.) every day for a total of seven injections. Tumor volume was measured with calipers, and blood was collected from the saphenous vein before the initial injection and the fourth injection. Mice were euthanized 4 hours after the last injection. For the long-term study in the LNCaP model (**Fig. 6F** and **G**), castration was performed when tumor diameter reached 7 to 8 mm. Mice were randomized and treated with JJ-450 (10 mg/kg body weight o.g., 10 mg/kg body weight i.p., or 75 mg/kg body weight o.g.) 6 days on, 1 day off, initiated 10 to 22 days after castration. Tumor volume was measured twice a week. For the 22Rv1 model (**Fig. 7A–C**), castration was performed when tumor diameter reached 5 mm. Mice were randomized and treated with JJ-450 (10 mg/kg body weight i.p., or 75 mg/kg body weight i.p.) every day, initiated at the time of castration. Tumor volume was measured 3 times a week. For the VCaP model (**Fig. 7D**), castration was performed when tumor volume reached approximately 250 mm^3. Mice were randomized and treated with JJ-450 (75 mg/kg body weight i.p.) or enzalutamide (10 mg/kg body weight i.p.) every day, initiated 2 weeks after castration. Animals displaying any signs of morbidity or ulceration of tumors were euthanized and removed from the study. Tumor volume was measured 3 times a week.

Transscrotal castration was performed under isoflurane anesthesia with proper aseptic and antiseptic technique (31). Mice were weighed weekly using a digital scale or a triple-beam balance, and blood was collected via saphenous vein or by cardiac puncture at euthanasia, and tumors were preserved for further biochemical and immunofluorescence analysis. Survival analysis was carried out using a tumor volume of 2,000 mm^3 as a surrogate for mortality and analyzed using GraphPad Prism 6.0 software (GraphPad Software). Statistical significance for the Kaplan–Meier analysis was determined using the log-rank (Mantel–Cox) test.

Small-molecule inhibitors

Small-molecule analogues of IMTPPE were synthesized as described previously (24). One active analogue (**325**) was conjugated to agarose (32) to generate beads (**403**) suitable for an AR pulldown assay. Two capped agarose beads (**403c**, **974**) were used as controls. The structures of these beads were provided in **Fig. 1A**. The chiral resolution of JJ-450 to give (−)-JJ-450 and (+)-JJ-450 was performed by chiral SCF chromatography. Doses were based on solubility data established for IMTPPE previously (23, 24).

AR pulldown assay

C4-2 cells cultured in complete RPMI medium in 15-cm dishes were used directly or transfected with desired plasmids for 48 hours prior to use for nuclear extract preparation. Cells were trypsinized, and cell pellets were resuspended with 1 mL TEDG buffer (1.5 mmol/L Tris-HCl, pH 7.4, 1 mmol/L EDTA, 1 mmol/L sodium molybdate, 1 mmol/L DTT, and 10% glycerol) with protease inhibitors. To collect nuclear extracts, cells were homogenized using a glass Dounce tissue homogenizer and centrifuged to pellet cell nuclei. Cell nuclei were washed and resuspended with TEDG buffer, followed by sonication. To collect whole cell extracts, cells were sonicated directly followed by centrifugation. Supernatant was transferred to a fresh tube. Control beads (30 μL) were used to preclear 500 μL lysates or purified AR in TEDG buffer. Beads were blocked using 2.5% BSA in PBS. Precleared cell lysates were diluted with TEDG buffer with protease inhibitor and incubated with beads at 4°C overnight. Beads were collected and washed with buffer (175 mmol/L NaCl, 20 mmol/L Tish-HCl, pH 7.5, 1% NP-40, 15% Glycerol, 1.5 mmol/L MgCl, 2 mmol/L EDTA) with

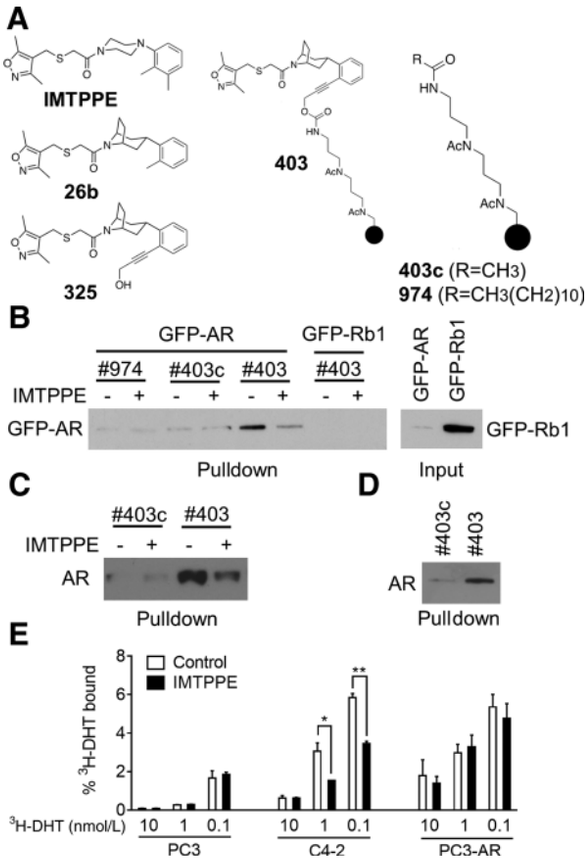

Figure 1.

IMTPPE scaffold directly binds to AR. **A,** Structures of IMTPPE, **26b**, **325**, and **325**-conjugated beads (**403**) and control beads (**403c** and **974**). **B,** GFP-AR, but not GFP-Rb1, was pulled down by **403**. C4-2 cells were transiently transfected with GFP-AR or GFP-Rb1 vectors for 48 hours in complete RPMI medium before collecting whole-cell lysates. Cell lysates were incubated with 50-fold IMTPPE or DMSO for 2 hours at room temperature prior to incubation with beads (**403**, **403c,** or **974**) at 4°C for 4 hours. The pulldown (left plot) and lysate input (right plot) were analyzed by immunoblot using anti-GFP antibody. **C,** C4-2 cells were cultured in complete RPMI medium with 1 nmol/L R1881 for nuclear extract preparation. Equal amount of nuclear extracts was incubated with agarose beads **403** or **403c** in the presence or absence of 50-fold IMTPPE at 4°C overnight. The pulldown samples were analyzed by immunoblot using anti-AR antibody. **D,** Purified AR protein was pulled down by **403**. Equal amount of human AR protein from Sigma was incubated with agarose beads **403** or **403c** at 4°C overnight. The pulldown samples were analyzed by immunoblot using anti-AR antibody. **E,** Effect of IMTPPE on DHT binding to AR in radioactive ligand-binding assay.^{3}H-DHT binding to AR in cytoplasmic extracts of C4-2 and PC3 cells stably transfected AR expression vector (PC3-AR) was determined in the presence of DMSO or 10 μmol/L IMTPPE at 4°C for overnight. Percentage of ^{3}H-DHT bound to AR in lysates was calculated. Cytoplasmic extracts of PC3 cells were served as control. Results represent mean ± SD and are representative of at least two biological replicates (*, $P < 0.05$ and **, $P < 0.01$).

protease inhibitors 3 times. Proteins were eluted with elution buffer (50 mmol/L $NaHCO_3$ and 1% SDS) at 4°C and denatured with SDS loading buffer, following immunoblotting analysis.

Radioactive ligand-binding assay

Cytoplasmic extracts were prepared using TEDG buffer for radioactive ligand-binding assay. The extracts were incubated with indicated concentrations of ^{3}H-DHT in the presence or absence of 10 μmol/L IMTPPE at 4°C overnight. Dextran-coated charcoal or Sephadex G25 columns were used to remove free ligand. ^{3}H-DHT in supernatant was measured using a scintillation counter. Percentage of ^{3}H-DHT bound to AR in lysate was calculated.

Plasmids and transfection

The expression vector pEGFP-C1 (Clontech) was used to generate GFP-AR or GFP-NAR (AR lacking LBD) as described previously (33). pEGFP-C1-ERα was kindly provided by Dr. Gerard Evan (34). *Renilla* luciferase reporter (pRL-TK) was purchased from Promega. PSA-luciferase reporter vector (pPSA6.1-Luc) was a kind gift provided by Dr. Marianne Sadar (35). Glucocorticoid receptor (GR) expression vector and MMTV-luciferase reporter were from Dr. Donald DeFranco (36). The 3X ERE TATA luc was a gift from Donald McDonnell (Addgene plasmid # 11354). pEGFP-C1-AR V7 was a gift from Michael Mancini and Marco Marcelli (Addgene plasmid # 86856). Plasmids were double CsCl gradient purified for transient transfection. Cell transfection was performed with PolyJet DNA In Vitro Transfection Reagent (SignaGen Laboratories) according to the manufacturer's protocols.

Western blot analysis

Cell lysates were prepared in RIPA buffer containing protease inhibitor cocktails (Sigma-Aldrich). Protein extract was boiled in SDS sample buffer, size fractionated by SDS-PAGE, and transferred onto a PVDF membrane (Bio-Rad). Membranes were blocked for 1 hour at room temperature in TBST buffer containing 5% nonfat milk and then incubated with the following primary antibodies overnight: anti-AR rabbit polyclonal (1:1,000, Santa Cruz Biotechnology, sc-816), anti-PSA goat polyclonal (1:500, Santa Cruz Biotechnology, sc-7638), anti-GFP rabbit polyclonal (1:1,000, Santa Cruz Biotechnology, SC-8334), anti-UBE2C rabbit polyclonal (1:1,000, Cell Signaling Technology, 14234S), and anti-GAPDH mouse monoclonal (1:10,000, Santa Cruz Biotechnology, sc-47724 HRP). After three washes in TBST, membranes were incubated with secondary antibody diluted in blocking buffer for 1 hour at room temperature. Following three washes in TBST, enhanced chemiluminescent (ECL) was performed using ECL Kit (Bio-Rad) and signals detected using ChemiDoc Imaging System (Bio-Rad).

qRT-PCR assays

To isolate RNA from cells, the RNeasy Mini Kit (Qiagen) was used following the manufacturer's protocol. To isolate RNA from xenograft tumors, tumor samples stored in RNAlater-ICE (Thermo Fisher Scientific) were homogenized in 600 μL lysis buffer using a digital ULTRA-TURRAX homogenizer (IKA-labortechnik). Samples were then centrifuged at 13,000 rpm/minute for 3 minutes. The supernatant was mixed with equal volume of 70% ethanol, and the RNA was further purified using the RNeasy Mini Kit (Qiagen). RNA was reverse transcribed using the PrimeScript RT Reagent Kit (TaKaRa). All reactions were performed in triplicated on an ABI StepOnePlus System (Applied Biosystems) using SYBR Advantage qPCR Premix (TaKaRa). The relative quantity of the target genes was calculated using the $\Delta\Delta C_t$ method by comparing average C_t of the target and mean C_t of the housekeeping gene, and GAPDH. Primer sequences are provided in Supplementary Table S1.

RNA-sequencing analysis

LNCaP cells were plated in 6-well plates with 5% charcoal-stripped FBS (cFBS) in phenol red–free RPMI medium (Corning) for 24 hours and then treated with ethanol or 1 nmol/L R1881 and

DMSO, IMTPPE (10 μmol/L), (−)-JJ-450 (10 μmol/L), enzalutamide (10 μmol/L), or (+)-JJ-450 (25 μmol/L) for an additional 24 hours in triplicate prior to total RNA isolation using an RNeasy Mini kit (Qiagen). RNA-Seq library construction and sequencing were performed by the Genomics Research Core of University of Pittsburgh. Libraries were prepared using the TruSeq Stranded mRNA Kit (Illumina) following the manufacturer's protocol. Briefly, starting from 1 μg total RNA, mRNA isolated from LNCaP cells was purified using oligo-dT magnetic beads. Following two rounds of purification, mRNA was fragmented. First strand reverse transcription was performed with random hexamer primers. After second strand synthesis, blunt-ended cDNA fragments were A-tailed followed by ligation of indexed sequencing adapters. PCR amplification provided selective enrichment of DNA with adapters ligated to both ends and was followed by library quantity and quality assessment using fluorometric assay (Qubit) and Agilent DNA 1000 TapeStation assay, respectively. Final libraries were normalized to 2 nmol/L, pooled, and diluted for instrument loading. Flow cells for the NextSeq 500 were seeded with 1.8 pmol/L denatured library for automated cluster formation and 2 × 75 paired-end sequencing. Sequencing generated between 42,985,974 and 56,182,970 pairs of reads for the 18 sequenced samples. FASTQC was run to examine the quality of the reads. Cutadapt v1.8.3 software was used for adapter trimming and quality trimming at a setting of 20 (37). The True Seq (Illumina) adapter sequences used for adapter trimming were AGATCGGAAGAGCACACGTCTGAACTCCAGTCA (left reads) and AGATCGGAAGAGCGTCGTGTAGGGAAAGAGTGT (right reads). Data analyses were performed by the Cancer Bioinformatics Services, a shared resource for UPMC Hillman researchers. Briefly, each sample was mapped to the Human Ensembl reference genome GRCh38 using the fast alignment tool HISAT2 v2.1.0 with default settings and library type set to RF (38). Transcripts in GRCh38 were quantified used HTSeq v0.9.0 using default settings for paired reads and library type set to reverse (39). An R Bioconductor package, edgeR, was used for differential gene analysis comparing drug treatment groups with a gene expression filter of > 1 CPM counts in at least three samples as expression above background (40). Heatmaps visualizing and comparing mRNA expression were generated using R.

Luciferase reporter assays

C4-2 or 22Rv1 cells were cotransfected with appropriate expression vectors and/or indicated report vectors in 5% cFBS, phenol red–free RPMI medium prior to treatment for 24 hours. GFP-ARv7: PC3 cells were cotransfected with pRL-TK and pPSA6.1-Luc report vectors in 5% cFBS, phenol red–free RPMI medium for 14 hours before treatment. After treatment, luciferase assays were performed as described previously (23). Briefly, cells were lysed and luciferase activity was assayed using a Dual-Luciferase Reporter Assay Kit (Promega) and measured using LMax II Microplate Reader (Molecular Devices) following the manufacturer's recommendations. The firefly luciferase activity was normalized to *Renilla* luciferase activity.

PSA ELISA assay

C4-2 cell culture medium supernatant was collected by centrifugation at 1,000 × *g* for 15 minutes at 4°C. Mouse serum was prepared by allowing blood samples to clot for 30 minutes at room temperature, followed by centrifugation at 1,000 × *g* for 15 minutes at 4°C. Culture medium supernatant and serum samples were stored at −80°C before ELISA assay. Total PSA level was measured using a Human Kallikrein 3/PSA Quantikine ELISA Kit (R&D) according to the manufacturer's protocols.

Chromatin immunoprecipitation

C4-2 cells were cultured in 5% cFBS, phenol red–free RPMI medium for 2 days, then treated with vehicle (ethanol) or 1 nmol/L R1881, combined with DMSO, 10 μmol/L IMTPPE, or JJ-450 for 2 hours. Cells were cross-linked using 1% paraformaldehyde for 10 minutes on a shaker at room temperature, and 0.125 mol/L glycine was used to stop cross-linking. After cross-linking, cells were washed and collected by centrifugation with cold PBS at 4°C. Cell pellets were lysed with cell lysis buffer (5 mmol/L PIPES, pH 8.0, 85 mmol/L KCl, and 0.5% NP40) plus 100X PMSF and100X PIC on ice for 10 minutes, and cell nuclei were pellet with centrifugation at 5,000 rpm for 5 minutes. Nuclei pellets were resuspended with nuclei lysis buffer (50 mmol/L Tris-Cl, pH 8.0, 10 mmol/L EDTA, and 1%SDS) plus 100X PMSF and 100X PIC. Sonication at desired intensity was used to shear chromatin to 200–1,000 bp fragments on ice. After preclearing with 20 μL salmon sperm DNA/Protein A agarose (EMD Millipore) at 4°C for 1 hour, the lysates were diluted in 10-fold with IP dilution buffer (0.01% SDS, 1.1% TritonX-100, 1.2 mmol/L EDTA, 16.7 mmol/L Tris-Cl, pH 8.1, and 167 mmol/L NaCL) and 50 μL diluted samples were saved as inputs. Anti-AR or rabbit IgG antibodies (4 μg) were added to each sample and incubated on a rotating platform at 4°C overnight. On the following day, 40 μL salmon sperm DNA/Protein A agarose was added for 2 hours. Agarose beads were washed with dialysis buffer (2 mmol/L EDTA, 50 mmol/L Tris-Cl, pH 8.0, and 0.2% Sarkosyl) 2 times and wash buffer (100 mmol/L Tris-Cl, pH 9.0, 500 mmol/L LiCl, 1% NP40, and 1% DOC) 4 times. The protein/DNA complexes were eluted with 50 mmol/L $NaHCO_3$ and 1% SDS at room temperature. All samples and inputs were incubated with 0.2 mol/L NaCl at 67°C overnight and then treated with RNase A and proteinase K. DNA was purified using QIAquick PCR Purification Kit (Qiagen) and amplified using SYBR Green PCR mix (Thermo Fisher Scientific) on an ABI StepOnePlus system (Applied Biosystems). Input chromatin was used for estimation of relative enrichment. Primer sequences for androgen-responsive elements (ARE) at regulatory regions of PSA and TMPRSS2 genes are provided in Supplementary Table S1.

IHC of xenografts

IHC staining for Ki67 was performed on LNCaP tumors subjected to short-term treatment using a standard protocol (41). Formalin-fixed, paraffin-embedded tissue sections were deparaffinized, and antigen retrieval was performed using antigen unmasking solution (Vector Laboratories) at 98°C to 100°C for 20 minutes. Endogenous peroxidase was inactivated by incubation with 1% hydrogen peroxide for 30 minutes at room temperature. Sections were then incubated sequentially in 1.5% blocking serum for 1 hour at room temperature, primary antibody [anti-Ki67 rabbit polyclonal (1:200, Abcam, ab15580), anti-cleaved caspase 3 rabbit monoclonal (1:100, Cell Signaling Technology, 9664S), or anti-AR rabbit monoclonal (1:100, CST, 5153S)] diluted in 1.5% serum at 4°C overnight, followed by incubation with biotinylated secondary anti-rabbit antibody (Santa Cruz Biotechnology) for 1 hour, AB enzyme reagent (avidin and biotinylated horseradish peroxidase; Santa Cruz Biotechnology) for 30 minutes at room temperature, followed by a 2- to 5-minute colorimetric development with peroxidase substrate kit (Vector Laboratories). Slides were counterstained with hematoxylin and mounted. Images of immunostained sections were acquired using a Leica DMLB microscope (Leica Microsystems Inc.). Ki67-positive cell density was determined by analysis of sections from at least eight different

xenografts from each group. Proliferative index was determined from five fields per tumor imaged at 20× magnification with no overlap, and Ki67-positive cells were counted to determine the average number of proliferating cells for each field. Positive cells were counted using Image-Pro Plus Software (Media Cybernetics).

Mice randomization and compounds administration

The randomization method used for each animal study was based on the tumor volume or diameter from fast to slow tumor growth: 1; 2; 3; 4; 4; 3; 2; 1; 1. . . etc. All compounds were dissolved in DMSO and then diluted with EtOH and Kolliphor-PBS with the ratio 1:1:8 and administered to mice by intraperitoneal injection or oral gavage.

Quantification and statistical analysis

Data are expressed as mean ± SD. Statistical significance, $P < 0.05$, was determined by two-tailed Student t test or log-rank Mantel–Cox test using GraphPad Prism 6.0 Software (GraphPad Software). The RNA-seq data in this article are deposited at Gene Expression Omnibus under accession number GSE115395.

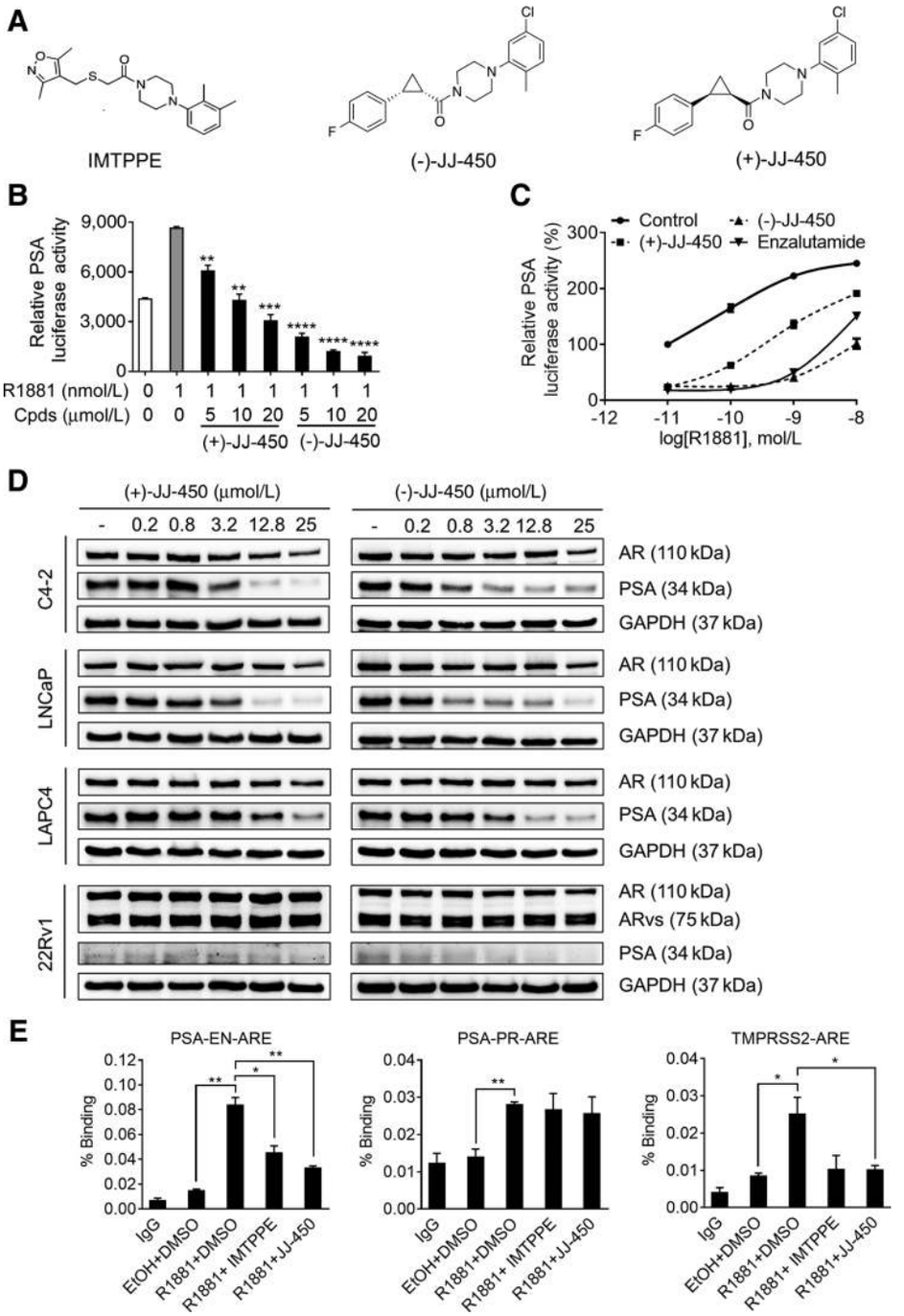

Figure 2.

JJ-450 inhibited AR recruitment to its target genes and AR transcriptional activity. **A,** Chemical structures of IMTPPE, (+)-JJ-450, and (−)-JJ-450. **B,** C4-2-PSA-rl cells (24), a C4-2 subline containing a PSA-luciferase reporter vector (pPSA6.1-Luc), and a *Renilla* luciferase reporter vector (pRL-TK), cultured in complete RPMI medium, were treated with 1 nmol/L R1881 in the presence of vehicle or indicated concentrations of (+)-JJ-450 or (−)-JJ-450 for 24 hours prior to luciferase assays. Firefly luciferase values were determined and normalized to Renilla. **C,** C4-2-PSA-rl cells were treated with indicated concentrations of R1881 in the presence of DMSO, 10 μmol/L (+)-JJ-450, (−)-JJ-450, or enzalutamide for 24 hours prior to luciferase assays. **D,** Western blot analysis of (−)-JJ-450 and (+)-JJ-450 inhibition of PSA expression in LNCaP, C4-2, LAPC4, and 22Rv1 cells. Cultured cells were treated with DMSO, (+)-JJ-450, or (−)-JJ-450 in complete RPMI/IMDM medium at indicated concentrations for 24 hours. GAPDH was probed as sample loading control. **E,** ChIP analysis of JJ-450 inhibition of R1881-induced AR binding to AREs in C4-2 cells. C4-2 cells were cultured with cFBS, phenol red–free RPMI medium and treated with 1 nmol/L R1881 and DMSO, 10 μmol/L IMTPPE, or JJ-450 for 2 hours before ChIP assays. JJ-450 and IMTPPE inhibited AR recruitment to the AREs in the PSA enhancer region (PSA-EN-ARE) and in TMPRSS2 promoter region, but not in the PSA promoter region (PSA-PR-ARE). Results represent mean ± SD and are representative of at least three biological replicates (*, $P < 0.05$; **, $P < 0.01$; ***, $P < 0.001$; and ****, $P < 0.0001$).

Results

IMTPPE directly binds to AR

IMTPPE was identified as a novel small molecule capable of inhibiting the nuclear localization and activity of AR in CRPC cells (22, 24). It was not clear, however, if IMTPPE exerts its effects by direct binding to AR. To test if the IMTPPE chemotype interacts directly with AR, small molecule–conjugated agarose beads (**403**) were developed for AR pulldown experiments, with an IMTPPE analogue and a linker suitable for an agarose attachment (**Fig. 1A**). The EC_{50} of **26b** in the PSA-luciferase assay is 7.9 ± 2.8 μmol/L, and the propargyl alcohol analogue **325** has an EC_{50} of 2.8 ± 1.0 (22). The linker containing analogue **404**, without conjugation to agarose beads, retained the ability to inhibit PSA-luciferase activity (Supplementary Fig. S1). Control beads included **403c** agarose beads and **974**-conjugated agarose beads (**Fig. 1A**). Transfected GFP-AR, but not GFP-Rb1, was pulled down by **403** beads, an effect that could be antagonized by IMTPPE (**Fig. 1B**). Similarly, endogenous AR in C4-2 cells was pulled down by **403** beads, but not by **403c** control beads, and IMTPPE could compete with the pulldown of AR by **403** beads (**Fig. 1C**). Furthermore, the **403** beads pulled down purified AR protein much more efficiently than #403c, which weakly pulled down the AR protein presumably due to nonspecific binding (**Fig. 1D**). Similar experiments to determine if JJ-450 could bind directly to AR were unsuccessful due to the low solubility of JJ-450. These results suggest that the IMTPPE scaffold could directly bind to AR.

Because IMTPPE could bind to AR directly, its effects on inhibiting androgen binding to AR were studied with radioactive ligand-binding assays of IMTPPE on ^{3}H-DHT binding to AR. In C4-2 cytoplasmic extracts, the percentage of bound ^{3}H-DHT decreased as the ^{3}H-DHT concentration increased from 0.1 to 10 nmol/L, becoming excessive as compared with AR (**Fig. 1E**). IMTPPE at 10 μmol/L reduced low-dose (0.1 and 1 nmol/L), but not high-dose (10 nmol/L) ^{3}H-DHT binding to AR in C4-2 cytoplasmic extracts (**Fig. 1E**). IMTPPE had no effect on ^{3}H-DHT binding to GFP-AR in PC3 cell extracts (**Fig. 1E**). These observations suggest IMTPPE could inhibit ligand binding to endogenous AR in AR-positive C4-2 cells but not in transfected GFP-AR in AR-negative PC3 cells.

JJ-450 inhibits AR transactivation of and recruitment to target genes

The effects of JJ-450 with enzalutamide on AR transcriptional activity were studied using a PSA-luciferase assay (24). JJ-450 is racemic and can be resolved into (−)-(1*S*,2*R*)-JJ-450 and (+)-(1*R*,2*S*)-JJ-450 (**Fig. 2A**; ref. 24). Both (−)-JJ-450 and (+)-JJ-450 inhibited the PSA-luciferase activity in a dose-dependent fashion in C4-2-PSA-rl cells, with (−)-JJ-450 being more potent than (+)-JJ-450 (**Fig. 2B** and **C**). In the PSA-luciferase assays using 10 μmol/L antagonists, enzalutamide was more effective at low concentrations of R1881 (0.1 nmol/L), whereas (−)-JJ-450 was more potent at higher concentrations of R1881 (1 and 10 nmol/L; **Fig. 2C**). This suggests that the mechanisms of AR inhibition by JJ-450 and enzalutamide are likely different.

The effects of JJ-450 on androgen induction of endogenous AR-target gene PSA at the protein level in LNCaP, C4-2, LAPC4, and 22Rv1 prostate cancer cells were also studied. Western blot analysis revealed that both (+)- and (−)-JJ-450 inhibited PSA protein levels, with (−)-JJ-450 being more potent in all the tested cell lines (**Fig. 2D**). Both (+)- and (−)-JJ-450 also inhibited AR expression levels slightly at 25 μmol/L (**Fig. 2D**). JJ-450 also inhibited normalized secreted PSA levels in the culture medium in a dose-dependent manner (Supplementary Fig. S2). qPCR analysis showed JJ-450 inhibition of R1881-induced mRNA expression of PSA (KLK3), EAF2, and NKX3.1, which are androgen-responsive genes (42), in LNCaP (Supplementary Fig. S3A), C4-2 (Supplementary Fig. S3B), VCaP (Supplementary Fig. S3C), and 22Rv1 (Supplementary Fig. S3D). However, the JJ-450 stereoisomers did not inhibit mRNA of either full-length AR (Supplementary Fig. S4A) or ARv7 (Supplementary Fig. S4B). These results suggest that JJ-450 could alter AR activity without reducing AR protein level.

To test whether IMTPPE or its analogues could also inhibit AR recruitment to AREs *in vivo*, chromatin immunoprecipitation (ChIP) assay was performed using the C4-2 cell line as a model. As expected, the synthetic androgen R1881 significantly increased AR binding to AREs (**Fig. 2E**). AR binding to AREs in the PSA gene enhancer (PSA-EN-ARE) and in the TMPRSS-2 gene (TMPRSS2-ARE) was significantly decreased by 10 μmol/L IMTPPE or its analogue JJ-450, but not ARE in the PSA promoter (PSA-PR-ARE; **Fig. 2E**). AR mRNA and protein expression levels were not inhibited by JJ-450 at this concentration (**Fig. 2D**; Supplementary Fig. S4A). These results suggest IMTPPE and its analogues could block AR recruitment to AREs.

JJ-450 inhibits ARv7 transcriptional activity and target gene expression

The inhibition of PSA expression in ARv7-positive 22Rv1 cells by (+)- and (−)-JJ-450 suggested that these compounds may also inhibit ARv7 or any AR variants/mutants lacking LBD, in addition to inhibiting full-length AR. In 22Rv1 cells, enzalutamide and JJ-450 stereoisomers showed a dose-dependent inhibition of PSA-luciferase activity in the presence of R1881 (**Fig. 3A**). JJ-450 stereoisomers, but not enzalutamide, inhibited PSA-luciferase activity in androgen-depleted conditions (**Fig. 3B**), suggesting that JJ-450 stereoisomers could inhibit ARv7 activity.

To further test JJ-450 inhibition of ARv7 and mutant AR lacking LBD, C4-2 cells were cotransfected with luciferase reporters along with GFP, GFP-AR-V7 (28), or GFP-NAR (AR mutant lacking LBD; ref. 33), followed by treatment with indicated compounds in androgen-depleted medium. In the absence of androgens, GFP-transfected C4-2 cells showed very low PSA-luciferase activity, whereas GFP-AR-V7– and GFP-NAR–transfected C4-2 cells exhibited robust luciferase activity (**Fig. 3C**). High concentrations of JJ-450 stereoisomers, but not enzalutamide, blocked PSA-luciferase induction by GFP-NAR or GFP-ARv7 (**Fig. 3C**). As a control, Western blot analysis showed no obvious change in transfected GFP, or GFP-ARv7, GFP-NAR protein levels in C4-2 cells (Supplementary Fig. S5A). Similarly, JJ-450 stereoisomers, but not enzalutamide, also inhibited PSA-luciferase induction by GFP-ARv7 in GFP-ARv7:PC3, a PC3 subline stably transfected with GFP-ARv7 (ref. 28; **Fig. 3D**). These results suggest that JJ-450 stereoisomers could target NTD and/or DBD domains in AR variants/mutants.

AR variant–mediated transcriptional programs appear to be different from ligand-induced AR-target genes (43, 44), so the effect of JJ-450 on ARv7-target gene expression in 22Rv1 cells cultured in the absence of androgens was studied. The 22Rv1 cell line is resistant to enzalutamide, due in part to the expression of AR variants (45). The mRNA levels of ARv7 signature genes, UBE2C, BUB1B, CCNA2, and KIF15 (43), were inhibited by JJ-450 stereoisomers at 20 μmol/L, but not by enzalutamide (**Fig. 3E**). Also, JJ-450 stereoisomers showed a dose-dependent inhibition of UBE2C protein expression, whereas enzalutamide showed minimal effect on UBE2C expression (**Fig. 3F**). Similarly, UBE2C, BUB1B, CCNA2, and KIF15 mRNA

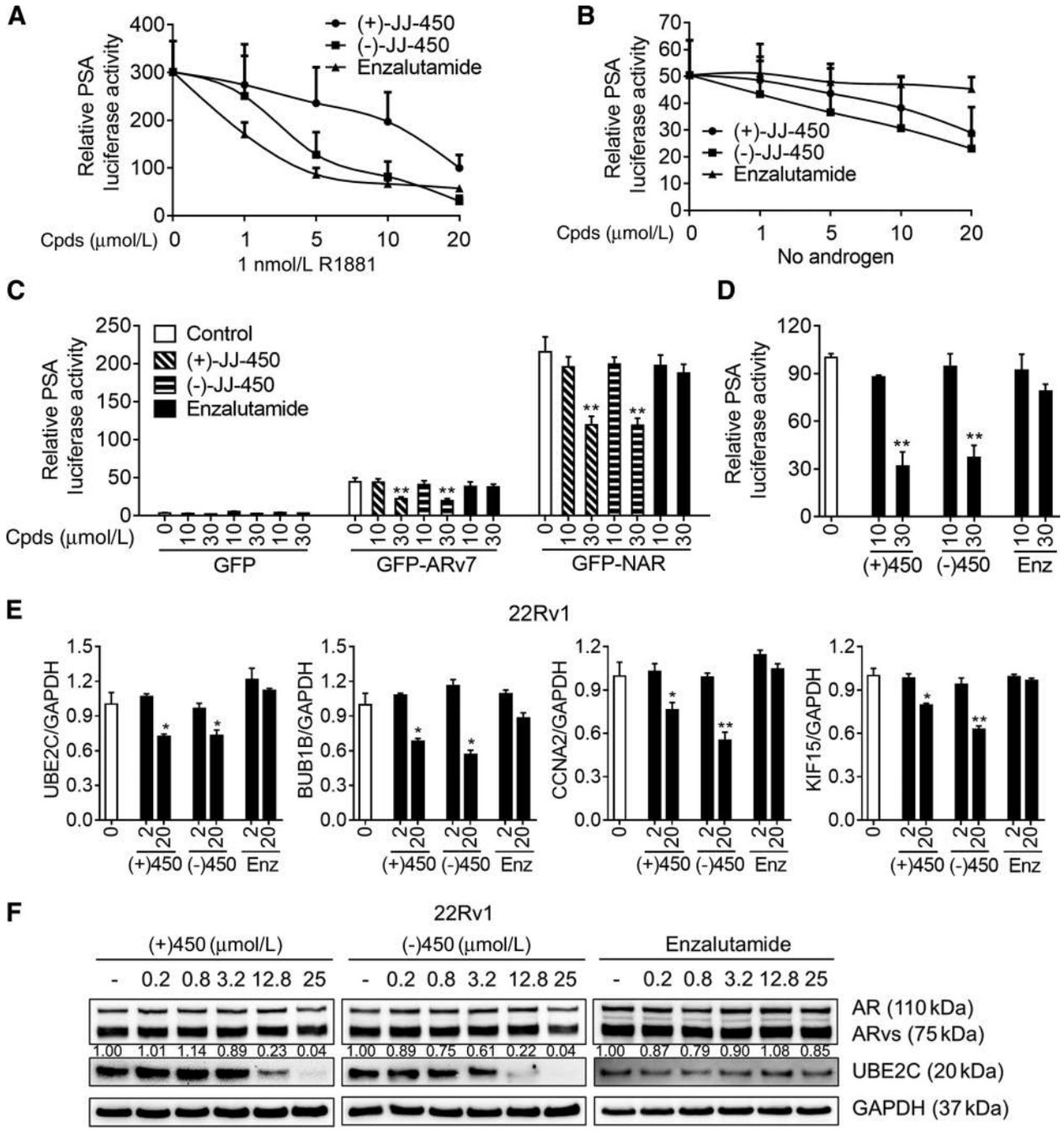

Figure 3.

JJ-450 inhibits LBD-independent transcriptional activity of AR. ARv7-positive 22Rv1 cells were transiently cotransfected with pPSA6.1-Luc and pRL-TK reporter vectors in cFBS, phenol red–free RPMI medium for 24 hours and then treated with indicated concentrations of (+)-JJ-450, (−)-JJ-450, or enzalutamide in the presence (**A**) or absence (**B**) of R1881 for additional 24 hours prior to luciferase assays. **C,** C4-2 cells were transiently transfected with pPSA6.1-Luc and pRL-TK reporter vectors, together with GFP, GFP-ARv7, or GFP-NAR (mutant AR lacking LBD) expression vectors for 24 hours in cFBS, phenol red–free RPMI medium, and then treated with indicated concentrations of (+)-JJ-450, (−)-JJ-450, or enzalutamide for additional 24 hours under androgen-depleted condition before luciferase assays. Parallel Western blot data were showed in Supplementary Fig. S5A. **D,** GFP-ARv7:PC3, a PC3 subline stably transfected GFP-ARv7 expression vector (28), was transiently cotransfected with pPSA6.1-Luc and pRL-TK reporter vectors for 14 hours in cFBS, phenol red–free RPMI medium, and then treated with indicated concentrations of (+)-JJ-450, (−)-JJ-450, or enzalutamide for additional 24 hours before luciferase assays. 22Rv1 cells were cultured in cFBS, phenol red–free RPMI medium for 24 hours, and then treated with indicated concentrations of (+)-JJ-450, (−)-JJ-450, or enzalutamide for additional 24 hours prior to qRT-PCR (**E**) or immunoblotting analysis (**F**). UBE2C protein expression was quantified relative to GAPDH for each lane using Image lab (Bio-Rad). The same experiment was also performed using another cell line CWR-R1 (Supplementary Fig. S5B). Results represent mean ± SD and are representative of at least three biological replicates (*, $P < 0.05$ and **, $P < 0.01$).

levels were also inhibited by JJ-450 stereoisomers in CWR-R1 cells under androgen-depleted condition (Supplementary Fig. S5B).

JJ-450 inhibition of AR

To determine whether JJ-450 could modify the action of other steroid nuclear receptors, the effect of JJ-450 on the transcriptional activities of estrogen receptor (ER) and GR using luciferase reporter assays in C4-2 cells was examined. ERα transactivation of 3× ERE TATA luciferase reporter (46) in the presence of 1 nmol/L 17β-estradiol (E2) was unaffected by JJ-450 (**Fig. 4A**). JJ-450 did not affect the protein levels of transfected GFP-ERα (**Fig. 4B**). Similarly, GR transactivation of MMTV-luciferase reporter (36) in the presence of 50 nmol/L dexamethasone was insensitive to JJ-450 (**Fig. 4C**), and JJ-450 did not affect GFP-GR protein levels (**Fig. 4D**). In C4-2 cells, 1 E2 and 50 nmol/L dexamethasone were sufficient to induce robust ERα and GR transcriptional activity (Supplementary Fig. S6A and S6B). These data suggest that JJ-450 could target AR specifically without affecting other steroid nuclear receptors.

To further evaluate the specificity of JJ-450 in the inhibition of AR function, RNA-seq analysis was performed with cultured LNCaP cells stimulated with R1881. In this study, LNCaP cells were cultured in androgen-depleted medium for 24 hours and then treated for an additional 24 hours with (i) vehicle, (ii) 1 nmol/L R1881, (iii) 1 nmol/L R1881 plus (−)-JJ-450, (iv) 1 nmol/L R1881 plus (+)-JJ-450, (v) 1 nmol/L R1881 plus IMTPPE, and (vi) 1 nmol/L R1881 plus enzalutamide. Differential expression (DE) genes were defined as those genes showing absolute fold change (FC) ≥ 2 and FDR ≤ 0.05. Multidimensional scaling (MDS) plots show the distinct cluster of samples with each treatment (**Fig. 5A**). The transcriptome of LNCaP cells treated with R1881 plus (−)-JJ-450 was very similar to R1881 plus enzalutamide, and both were similar to the vehicle control. The transcriptome of LNCaP cells treated with R1881 plus IMTPPE and R1881 plus (+)-JJ-450 appeared to be similar to each other, but was different from the vehicle or the R1881-only group (**Fig. 5A**). The gene expression profiles were also analyzed using unsupervised clustering, and a heatmap was generated which included 13,490 DE genes. Consistent with the MDS analysis, a heatmap showed that most gene expression changes induced by R1881 were repressed by (−)-JJ-450 or enzalutamide (**Fig. 5B**), whereas (+)-JJ-450 and IMTPPE could repress part of the R1881-induced gene expression program and induce DE of several/many additional genes (**Fig. 5B**). Compared with R1881 plus enzalutamide, R1881 plus IMTPPE and R1881 plus (+)-JJ-450 induced 2,856 and 2,878 DE genes, respectively (**Fig. 5C**; Supplementary Table S2). There were 186 DE genes between R1881 plus enzalutamide and the vehicle control, and only 56 DE genes between R1881 plus (−)-JJ-450 and the vehicle control (**Fig. 5D**; Supplementary Table S3). As anticipated, R1881 induced significant changes in transcripts previously identified as androgen-response genes. A heatmap generated for 25 androgen-responsive genes also verified that our compounds inhibited the expression of AR-regulated genes, with (−)-JJ-450 having similar specificity as enzalutamide (Supplementary Fig. S7). These data indicate (−)-JJ-450 could inhibit R1881 activation of AR completely, with specificity and potency similar to enzalutamide.

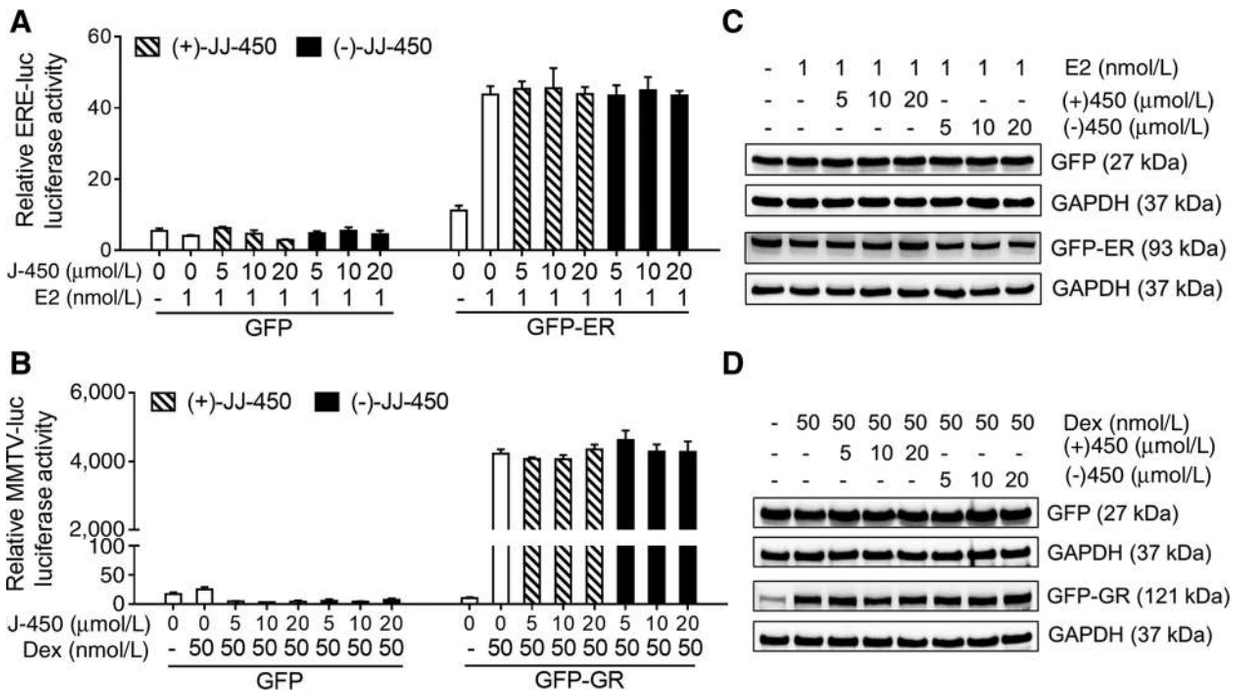

Figure 4.

(−)-JJ-450 and (+)-JJ-450 do not inhibit ERα or GR in C4-2 cells. C4-2 cells were transiently cotransfected with Renilla luciferase reporter and 3x-ERE-TATA luciferase reporter (46), together with GFP or GFP-ERα expression vectors for 24 hours in cFBS, phenol red–free RPMI medium, and then treated with 1 nmol/L 17β-estradiol (E2) and indicated concentrations of (+)-JJ-450 or (−)-JJ-450 for additional 24 hours for luciferase assays (**A**) or Western blot (**B**). Similarly, C4-2 cells were transiently cotransfected with Renilla luciferase reporter and MMTV-firefly luciferase reporter (36), together with GFP or GFP-GR expression vectors for 24 hours in cFBS, phenol red–free RPMI medium, and then treated with 50 nmol/L dexamethasone (Dex) and indicated concentrations of (+)-JJ-450/(−)-JJ-450 for additional 24 hours for luciferase assay (**C**) or Western blot (**D**). Results represent mean ± SD and are representative of at least three biological replicates.

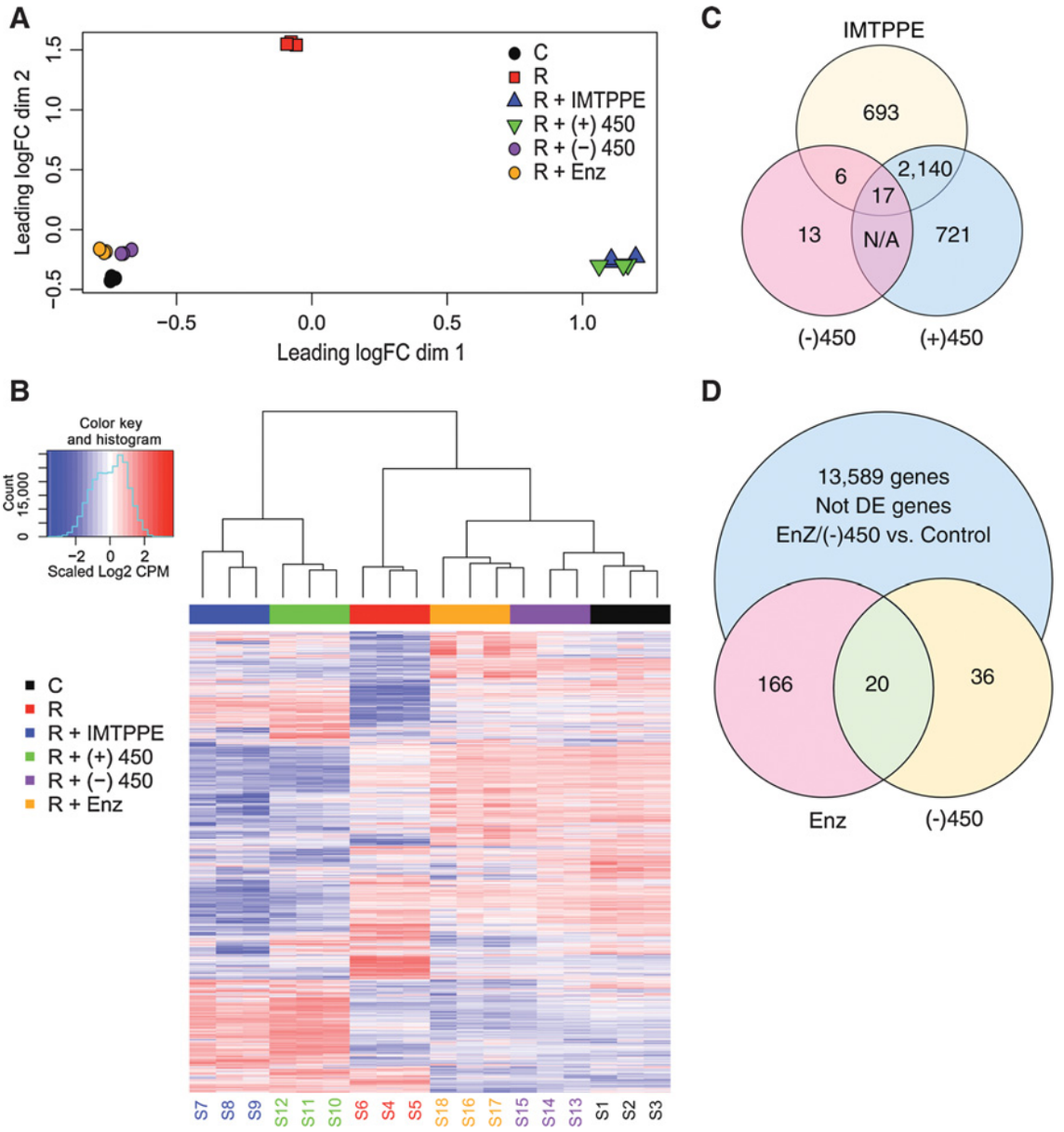

Figure 5.

(−)-JJ-450 inhibits AR-dependent transcriptome specifically. RNA-seq analysis was performed to determine the effect IMTPPE, (−)-JJ-450, (+)-JJ-450, and enzalutamide on R1881-induced transcriptome in cultured LNCaP cells. Differentially expressed genes were defined as those showing absolute FC $\geq$2 and FDR $\leq$ 0.05. R, R1881; (+)450, (+)-JJ-450; (−)450, (−)-JJ-450; Enz, Enzalutamide. **A,** MDS analysis of the whole gene expression program. **B,** Heatmap of the whole gene expression program. Heatmap of selected 25 androgen-responsive genes was provided in Supplementary Fig. S7. **C,** Venn diagram analysis of DE genes among three groups: enzalutamide versus IMTPPE, enzalutamide versus. (+)-JJ-450, and enzalutamide versus (−)-JJ-450. More details are provided in Supplementary Table S2. **D,** Venn diagram analysis of genes expression between two groups: control versus enzalutamide and control versus (−)-JJ-450. More details are provided in Supplementary Table S3. Experiments were performed on three biological replicates for each group.

JJ-450 inhibition of AR in relapsed LNCaP xenograft prostate tumors

In xenograft tumor experiments, the racemic mixture of JJ-450 was used to reduce the number of animals and quantity of compound required. FDA-approved bicalutamide is currently used as a racemic mixture for prostate cancer treatment (47, 48); therefore, using a racemic mixture of JJ-450 in animal studies has potential clinical relevance. Mice bearing subcutaneous LNCaP tumor xenografts were castrated when tumor volume reached approximately 200 mm^3. After tumors relapsed and reached a volume of approximately 300 mm^3, mice were randomized and intraperitoneally injected with vehicle, enzalutamide (10 mg/kg body weight), or JJ-450 (25 mg/kg body weight) every day for a total of seven injections. Both enzalutamide and JJ-450 inhibited growth of relapsed LNCaP tumors, serum PSA level

normalized to tumor volume, and tumor proliferation marker Ki67 as compared with vehicle (**Fig. 6A–D**). mRNAs of two AR-target genes, PSA and FKBP5, were also inhibited by J-450 and enzalutamide (**Fig. 6E**). However, JJ-450 and enzalutamide did not affect caspase-3 immunostaining or the AR level and nuclear localization in relapsed LNCaP tumors (**Fig. 6C**).

To further verify the effect on relapsed LNCaP xenografts, mice with subcutaneous LNCaP xenografts were castrated when tumor diameter reached 7 to 8 mm and treated long-term with JJ-450 at indicated dosages with either oral gavage or intraperitoneal injection, 6 days on, 6 day off, started 10 days after castration (**Fig. 6F**). All the JJ-450 treatment regimens inhibited the LNCaP tumor growth as compared with the vehicle-treated mice (**Fig. 6F**). Median survival times treated with JJ-450 10 mg/kg body weight o.g, 10 mg/kg body weight i.p., and 75 mg/kg body weight o.g. were 47, 55, and 54 days, respectively, significantly longer than the median survival time (39 days) of vehicle group (**Fig. 6G**). These results suggest that JJ-450 could block AR function *in vivo* and inhibit tumor growth of relapsed LNCaP tumors.

JJ-450 inhibition of CRPC xenograft tumors that express AR splice variants

The effect of JJ-450 on CRPC tumors that express full-length AR and AR variants was evaluated using the 22Rv1 and VCaP xenograft tumor models (49–53). The 22Rv1 tumor volume in animals treated with JJ-450 was reduced by more than 60% compared with the vehicle-treated group at both low (10 mg/kg body weight) and high (75 mg/kg body weight) doses (**Fig. 7A**). Median survival time for animals treated with JJ-450 was 43 and 49 days, at low and high doses respectively, which was significantly longer than the median survival time of 25 days for the vehicle control groups (**Fig. 7B**). Mice treated with JJ-450 showed no changes in body weight (**Fig. 7C**). Tumor growth of VCaP xenografts was also significantly reduced by JJ-450, and JJ-450 was more potent than enzalutamide (**Fig. 7D**). These results suggest that JJ-450 could inhibit CRPC xenografts expressing AR variants *in vivo*.

Discussion

The present study provides evidence that JJ-450 represents a novel class of AR antagonists capable of inhibiting both full-length AR and AR splice variants lacking LBD. These results show this class of small molecules can directly bind to AR, block AR recruitment to AREs, and inhibit AR-target gene expression, including those induced by AR splice variants. Furthermore, JJ-450 could inhibit the growth of several AR-positive xenograft prostate tumor models, including enzalutamide-resistant 22Rv1 tumors.

In the RNA-seq study, (−)-JJ-450 inhibition of AR-target genes was almost identical to enzalutamide, which is a superb AR antagonist with high specificity (8). This finding together with the pulldown of purified AR by a JJ-450 and IMTPPE analogue, **403**, strongly argues that JJ-450 targets AR directly and specifically. Thus, the JJ-450 chemotype could be used to develop a new class of highly specific AR antagonists.

Although both enzalutamide and JJ-450 exhibited similar specificity in AR inhibition based on the RNA-seq analysis in the LNCaP model, these two small molecules bind to different sites on AR. Enzalutamide and all the other FDA-approved AR antagonists target the LBD of AR, and they do not affect AR splice variants or AR mutants lacking LBD. In contrast, JJ-450 and its analogues could inhibit full-length AR, ARv7, and NAR, a mutant AR that lacks LBD, suggesting that JJ-450 inhibition of AR was mediated through the NTD and/or DBD. IMTPPE had no effect on ^{3}H-DHT binding to transfected GFP-AR in AR-negative PC3 cells (see **Fig. 1E**), suggesting that IMTPPE does not influence DHT for binding to the LBD of GFP-AR in PC3 cells. However, IMTPPE could bind to other domain(s) of AR such as NTD and/or DBD to inhibit PSA-luciferase induction by GFP-ARv7 in PC3: GFP-ARv7 (see **Fig. 3D**), which contains NTD and DBD, but lacks LBD. However, we cannot rule out the possibility that JJ-450 may also interact with LBD, because it inhibited DHT binding to AR in C4-2 cells. However, JJ-450 did not inhibit DHT binding to transfected GFP-AR in PC3 cells. One possible explanation is that AR is hypersensitized to DHT in C4-2 cells (27) but not in PC3 cells, and JJ-450 may inhibit AR hypersensitization via targeting the NTD of AR. Another possibility is that the AR in C4-2 is mutated (54), whereas transfected GFP-AR in PC3 is wild-type. Future experiments will be required to conclusively determine whether IMTPPE and JJ-450 directly interact with AR, and further studies will be needed to address why JJ-450 inhibited DHT binding to AR in C4-2 cells but not to GFP-AR in PC3 cells.

The studies using the LNCaP xenograft tumor model show that JJ-450 can suppress AR function *in vivo*. JJ-450 suppresses serum PSA normalized to tumor volume in mice bearing LNCaP tumors, indicating that JJ-450 suppresses PSA synthesis on a per cell basis in LNCaP tumors. This is further supported by JJ-450 suppression of PSA mRNA expression in LNCaP tumors. Taken together, these findings suggest that JJ-450 inhibition of LNCaP tumor growth is mediated through AR inhibition.

In this study, JJ-450 inhibited AR-positive xenograft prostate tumors, including 22Rv1 xenograft tumors which express ARv7 and are resistant to LBD-targeting AR antagonists including enzalutamide (45). In our experiments, JJ-450 appeared to inhibit LNCaP xenografts more effectively than 22Rv1 xenografts (see **Figs. 6F** and **7A**). This difference may reflect that AR in LNCaP can be more effectively inhibited by JJ-450 than the AR in 22Rv1. 22Rv1 cells express both full-length AR and AR splice variants including ARv7 that lacks LBD. **Figure 3C** showed that JJ-450 at high dose (30 μmol/L), but not low dose (10 μmol/L), inhibited ARv7 activity. Thus, JJ-450 inhibition of ARvs may not be as potent as its inhibition of full-length AR. One major reason for 22Rv1 being less sensitive to JJ-450 than LNCaP is likely that 22Rv1, but not LNCaP, cells express ARvs (55, 56). According to the literature, enzalutamide can inhibit LNCaP but not 22Rv1 xenograft (57, 58). It is thought that ARvs in 22Rv1 are responsible for the resistance to enzalutamide (45). JJ-450 and enzalutamide may target different domains of AR, and the mechanisms leading to enzalutamide resistance may not confer JJ-450 resistance. Accordingly, it might be feasible to further develop JJ-450 to treat metastatic CRPC resistant to enzalutamide. Because JJ-450 and enzalutamide target different regions in AR, the combination of JJ-450 with enzalutamide or any LBD-targeting AR antagonist could be synergistic, and it may be more difficult for AR to develop simultaneous resistance to both JJ-450 and enzalutamide.

In summary, this work suggests that JJ-450 is a promising clinical lead compound for the future development of a new class of AR antagonists that can target AR and AR splice variants lacking LBD. Further studies should focus on the determining whether JJ-450 analogues and AR directly interact, development of JJ-450 analogues that have sufficient oral bioavailability and favorable pharmacokinetics, as well as mechanistic studies defining the exact binding site(s) of JJ-450 on AR.

Disclosure of Potential Conflicts of Interest

P. Wipf reports receiving a commercial research grant from UPMC Enterprises. Z. Wang reports receiving a commercial research grant from UPMC Enterprises

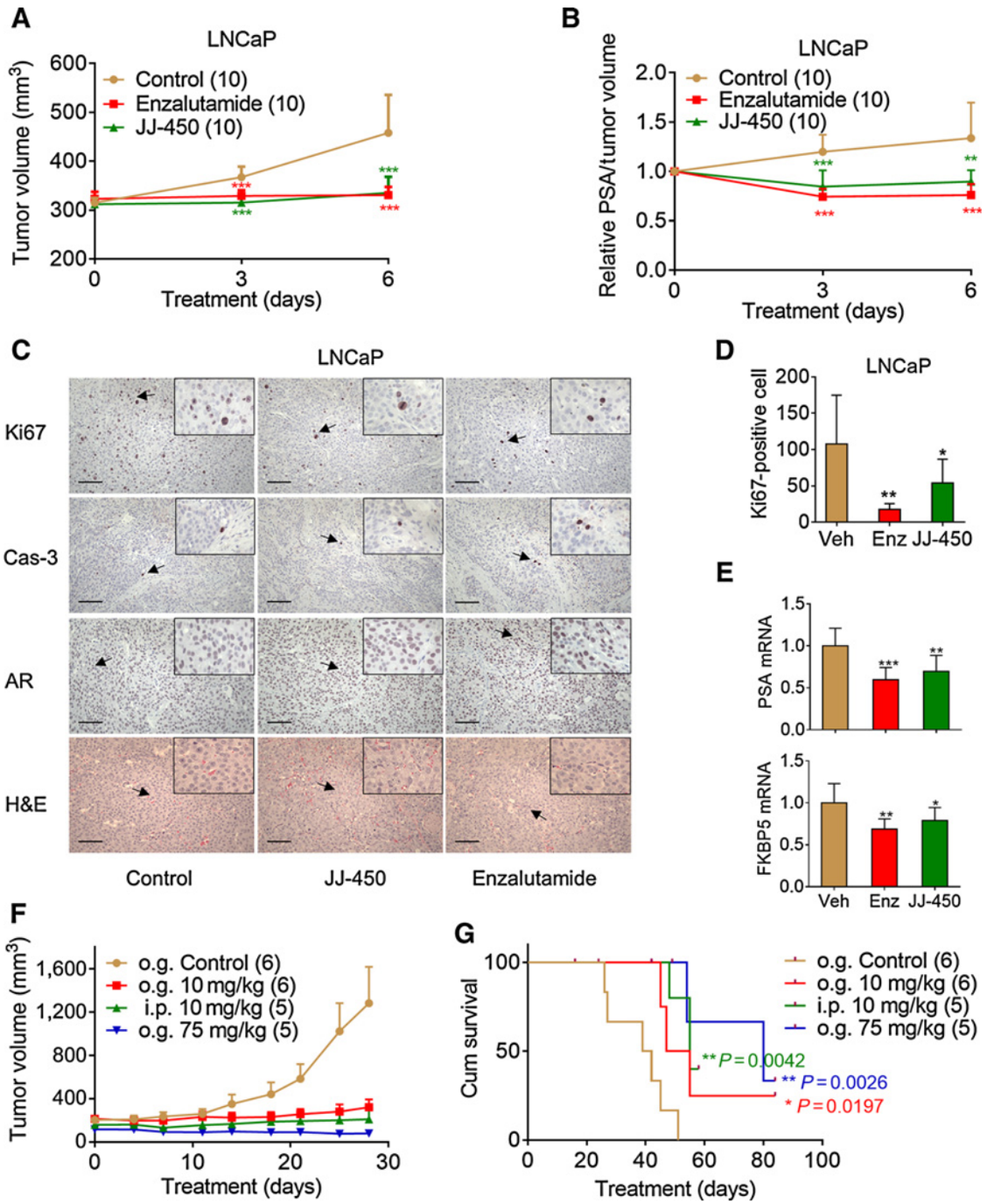

Figure 6.

JJ-450 inhibited growth and expression of AR-target genes in relapsed LNCaP xenograft tumors in castrated mice. JJ-450 or enzalutamide inhibited the short-term growth of relapsed LNCaP tumors (**A**) and serum PSA normalized to tumor volume in mice (**B**) at days 3 and 6 after the treatment. **C,** Representative IHC images of LNCaP xenografts in **A** and stained for Ki67, cleaved caspase-3 (Cas-3), AR, and hematoxylin and eosin (H&E). Scale bars, 100 μm. **D,** Ki-67–positive cell density was determined for LNCaP xenograft tumors. JJ-450 and enzalutamide significantly reduced proliferation compared with control. Student *t* test. Mean ± SD. **E,** Relative PSA and FKBP5 mRNA level in xenografts at day 6. **F,** JJ-450 inhibited long-term growth of relapsed LNCaP xenograft tumors in castrated mice. Castration was performed when LNCaP xenograft tumor diameter reached to 7 to 8 mm. Mice were randomized and treated with JJ-450 (10 mg/kg body weight o.g., 10 mg/kg body weight i.p., 75 mg/kg body weight o.g.) 6 days on, 1 day off, started 10 to 22 days after castration. Mean ± SD. **G,** Kaplan–Meier curves of mice described in **F** showing the effect of JJ-450 on the survival of LNCaP tumor–bearing mice. Significance was determined using a Log-rank Mantel–Cox test. Results represent mean ± SD, and number of animals indicated in parentheses. *, $P < 0.05$; **, $P < 0.01$; and ***, $P < 0.001$. Enz, enzalutamide.

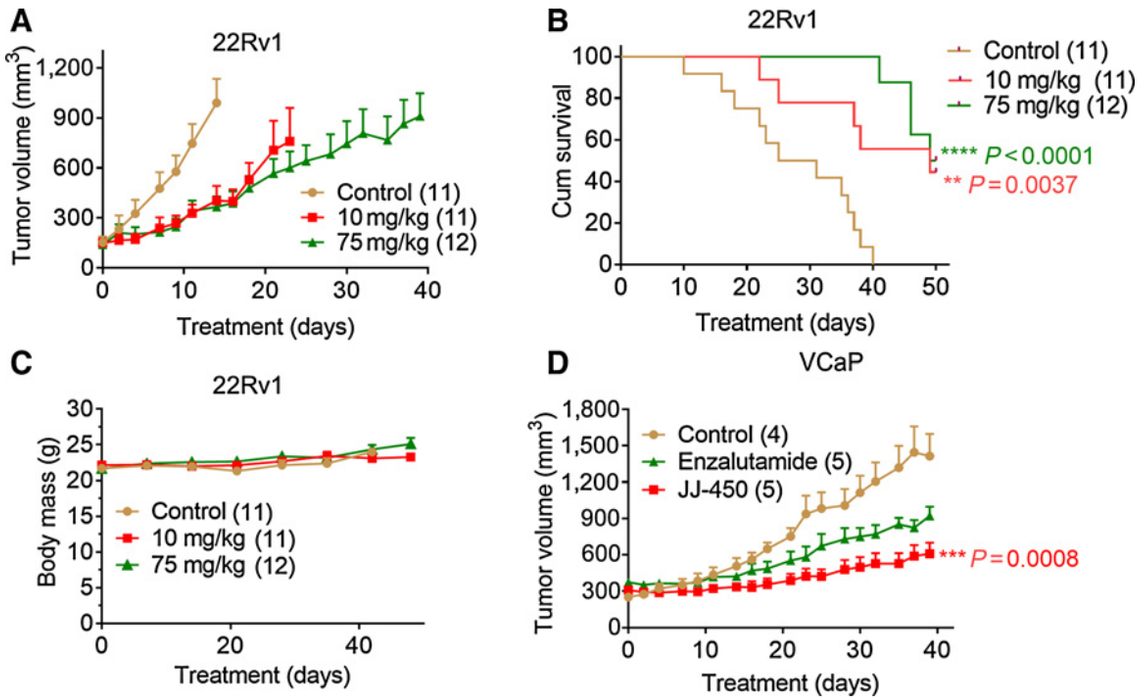

Figure 7.

JJ-450 inhibited growth of relapsed xenograft tumors that express AR splice variants in castrated mice. **A,** Mice with 22Rv1 xenograft were castrated when tumor diameter reached to 5 mm. Mice were randomized and treated with JJ-450 (10 mg/kg body weight i.p. and 75 mg/kg body weight i.p.) every day at the time of castration. **B,** Body weight of animals described in **A** over the duration of the experiment. **C,** Kaplan–Meier curves of mice described in **A** showing the effect of JJ-450 on the survival of 22Rv1 tumor–bearing mice. Significance was determined using a Log-rank Mantel–Cox test. **D,** Mice with VCaP xenograft were castrated when tumor volume reached to approximately 250 mm^3. Mice were randomized and treated with JJ-450 (75 mg/kg body weight i.p.) or enzalutamide (10 mg/kg body weight i.p.) every day, started 2 weeks after castration. Results represent mean ± SD, and number of animals indicated in parentheses.

and has an ownership interest in US Patent. No potential conflicts of interest were disclosed by the other authors.

Authors' Contributions

Conception and design: D. Wang, J.K. Johnson, J.B. Nelson, P. Wipf, Z. Wang
Development of methodology: Z. Yang, D. Wang, J.K. Johnson, P. Wipf, Z. Wang
Acquisition of data (provided animals, acquired and managed patients, provided facilities, etc.): Z. Yang, D. Wang, J.K. Johnson, L.E. Pascal, K. Takubo, J. Zhou, W. Chen, M. Zhong, Q. Song, H. Ding, Z. Wu, P. Wipf, Z. Wang
Analysis and interpretation of data (e.g., statistical analysis, biostatistics, computational analysis): Z. Yang, D. Wang, L.E. Pascal, K. Takubo, R. Avula, A. B. Chakka, U.R. Chandran, P. Wipf, Z. Wang
Writing, review, and/or revision of the manuscript: Z. Yang, D. Wang, J.K. Johnson, L.E. Pascal, U.R. Chandran, T.S. Maskrey, P. Wipf, Z. Wang
Administrative, technical, or material support (i.e., reporting or organizing data, constructing databases): Z. Yang, J. Zhou, M. Zhong, T.S. Maskrey, Z. Wang
Study supervision: T.S. Maskrey, J.B. Nelson, P. Wipf, Z. Wang

Acknowledgments

This work was funded in part by DOD Award W81XWH-16-1-0659; by NIH grants R01 CA186780 (to Z. Wang), P50 CA180995 (to Z. Wang), and R50 CA211242 (to L.E. Pascal) as well as by UPMC Enterprises. This project used the UPMC Hillman Cancer Center Animal Facility, the Tissue and Research Pathology Services/Pitt Biospecimen Core, and the Genomics Research Core, and Cancer Bioinformatics Services which were supported in part by NCI award P30 CA047904 and the Senior Vice Chancellor's Office at University of Pittsburgh. We are grateful to Megan Lambert, Robin Frederick, and Aiyuan Zhang for technical support.

The costs of publication of this article were defrayed in part by the payment of page charges. This article must therefore be hereby marked *advertisement* in accordance with 18 U.S.C. Section 1734 solely to indicate this fact.

Received May 7, 2019; revised August 8, 2019; accepted September 17, 2019; published first September 25, 2019.

References

1. Siegel RL, Miller KD, Jemal A. Cancer statistics, 2018. CA Cancer J Clin 2018;68:7–30.
2. Zegarra-Moro OL, Schmidt LJ, Huang H, Tindall DJ. Disruption of androgen receptor function inhibits proliferation of androgen-refractory prostate cancer cells. Cancer Res 2002;62:1008–13.
3. Chen CD, Welsbie DS, Tran C, Baek SH, Chen R, Vessella R, et al. Molecular determinants of resistance to antiandrogen therapy. Nat Med 2004;10:33–9.
4. Agoulnik IU, Vaid A, Bingman WE III, Erdeme H, Frolov A, Smith CL, et al. Role of SRC-1 in the promotion of prostate cancer cell growth and tumor progression. Cancer Res 2005;65:7959–67.
5. Knudsen KE, Scher HI. Starving the addiction: new opportunities for durable suppression of AR signaling in prostate cancer. Clin Cancer Res 2009;15:4792–8.
6. Mohler JL. Castration-recurrent prostate cancer is not androgen-independent. Adv Exp Med Biol 2008;617:223–34.
7. Attard G, Reid AH, A'Hern R, Parker C, Oommen NB, Folkerd E, et al. Selective inhibition of CYP17 with abiraterone acetate is highly active in the treatment of castration-resistant prostate cancer. J Clin Oncol 2009;27:3742–8.
8. Tran C, Ouk S, Clegg NJ, Chen Y, Watson PA, Arora V, et al. Development of a second-generation antiandrogen for treatment of advanced prostate cancer. Science 2009;324:787–90.

9. Clegg NJ, Wongvipat J, Joseph JD, Tran C, Ouk S, Dilhas A, et al. ARN-509: a novel antiandrogen for prostate cancer treatment. Cancer Res 2012;72:1494–503.
10. Smith MR, Saad F, Chowdhury S, Oudard S, Hadaschik BA, Graff JN, et al. Apalutamide treatment and metastasis-free survival in prostate cancer. N Engl J Med 2018;378:1408–18.
11. Moilanen AM, Riikonen R, Oksala R, Ravanti L, Aho E, Wohlfahrt G, et al. Discovery of ODM-201, a new-generation androgen receptor inhibitor targeting resistance mechanisms to androgen signaling-directed prostate cancer therapies. Sci Rep 2015;5:12007.
12. Beer TM, Armstrong AJ, Rathkopf DE, Loriot Y, Sternberg CN, Higano CS, et al. Enzalutamide in metastatic prostate cancer before chemotherapy. N Engl J Med 2014;371:424–33.
13. de Bono JS, Logothetis CJ, Molina A, Fizazi K, North S, Chu L, et al. Abiraterone and increased survival in metastatic prostate cancer. N Engl J Med 2011;364:1995–2005.
14. Scher HI, Fizazi K, Saad F, Taplin ME, Sternberg CN, Miller K, et al. Increased survival with enzalutamide in prostate cancer after chemotherapy. N Engl J Med 2012;367:1187–97.
15. Boudadi K, Antonarakis ES. Resistance to novel antiandrogen therapies in metastatic castration-resistant prostate cancer. Clin Med Insights Oncol 2016;10:1–9.
16. Yuan X, Cai C, Chen S, Chen S, Yu Z, Balk SP. Androgen receptor functions in castration-resistant prostate cancer and mechanisms of resistance to new agents targeting the androgen axis. Oncogene 2014;33:2815–25.
17. Watson PA, Arora VK, Sawyers CL. Emerging mechanisms of resistance to androgen receptor inhibitors in prostate cancer. Nat Rev Cancer 2015;15:701–11.
18. Prekovic S, Van den Broeck T, Linder S, van Royen ME, Houtsmuller A, Handle F, et al. Molecular underpinnings of enzalutamide resistance. Endocr Relat Cancer 2018;25:R545–57.
19. Andersen RJ, Mawji NR, Wang J, Wang G, Haile S, Myung JK, et al. Regression of castrate-recurrent prostate cancer by a small-molecule inhibitor of the amino-terminus domain of the androgen receptor. Cancer Cell 2010;17:535–46.
20. Dalal K, Roshan-Moniri M, Sharma A, Li H, Ban F, Hassona MD, et al. Selectively targeting the DNA-binding domain of the androgen receptor as a prospective therapy for prostate cancer. J Biol Chem 2014;289:26417–29.
21. Ponnusamy S, Coss CC, Thiyagarajan T, Watts K, Hwang DJ, He Y, et al. Novel selective agents for the degradation of androgen receptor variants to treat castration-resistant prostate cancer. Cancer Res 2017;77:6282–98.
22. Johnston PA, Nguyen MM, Dar JA, Ai J, Wang Y, Masoodi KZ, et al. Development and implementation of a high-throughput high-content screening assay to identify inhibitors of androgen receptor nuclear localization in castration-resistant prostate cancer cells. Assay Drug Dev Technol 2016;14:226–39.
23. Masoodi KZ, Eisermann K, Yang Z, Dar JA, Pascal LE, Nguyen M, et al. Inhibition of androgen receptor function and level in castration-resistant prostate cancer cells by 2-[(isoxazol-4-ylmethyl)thio]-1-(4-phenylpiperazin-1-yl)ethanone. Endocrinology 2017;158:3152–61.
24. Johnson JK, Skoda EM, Zhou J, Parrinello E, Wang D, O'Malley K, et al. Small molecule antagonists of the nuclear androgen receptor for the treatment of castration-resistant prostate cancer. ACS Med Chem Lett 2016;7:785–90.
25. Wu HC, Hsieh JT, Gleave ME, Brown NM, Pathak S, Chung LW. Derivation of androgen-independent human LNCaP prostatic cancer cell sublines: role of bone stromal cells. Int J Cancer 1994;57:406–12.
26. Klein KA, Reiter RE, Redula J, Moradi H, Zhu XL, Brothman AR, et al. Progression of metastatic human prostate cancer to androgen independence in immunodeficient SCID mice. Nat Med 1997;3:402–8.
27. Gregory CW, Johnson RT Jr, Mohler JL, French FS, Wilson EM. Androgen receptor stabilization in recurrent prostate cancer is associated with hypersensitivity to low androgen. Cancer Res 2001;61:2892–8.
28. Szafran AT, Stephan C, Bolt M, Mancini MG, Marcelli M, Mancini MA. High-content screening identifies Src family kinases as potential regulators of AR-V7 expression and androgen-independent cell growth. Prostate 2017;77:82–93.
29. Wang D, Nguyen MM, Masoodi KZ, Singh P, Jing Y, O'Malley K, et al. Splicing factor Prp8 interacts with NES(AR) and regulates androgen receptor in prostate cancer cells. Mol Endocrinol 2015;29:1731–42.
30. Euhus DM, Hudd C, LaRegina MC, Johnson FE. Tumor measurement in the nude mouse. J Surg Oncol 1986;31:229–34.
31. Wang Y, Gupta S, Hua V, Ramos-Garcia R, Shevrin D, Jovanovic BD, et al. Prolongation of off-cycle interval by finasteride is not associated with survival improvement in intermittent androgen deprivation therapy in LNCaP tumor model. Prostate 2010;70:147–54.
32. Wang X, Imber BS, Schreiber SL. Small-molecule reagents for cellular pull-down experiments. Bioconjug Chem 2008;19:585–7.
33. Saporita AJ, Zhang Q, Navai N, Dincer Z, Hahn J, Cai X, et al. Identification and characterization of a ligand-regulated nuclear export signal in androgen receptor. J Biol Chem 2003;278:41998–2005.
34. Littlewood TD, Hancock DC, Danielian PS, Parker MG, Evan GI. A modified oestrogen receptor ligand-binding domain as an improved switch for the regulation of heterologous proteins. Nucleic Acids Res 1995;23:1686–90.
35. Sadar MD. Androgen-independent induction of prostate-specific antigen gene expression via cross-talk between the androgen receptor and protein kinase A signal transduction pathways. J Biol Chem 1999;274:7777–83.
36. Dekelbab BH, Witchel SF, DeFranco DB. TNF-alpha and glucocorticoid receptor interaction in L6 muscle cells: a cooperative downregulation of myosin heavy chain. Steroids 2007;72:705–12.
37. Martin M. Cutadapt removes adapter sequences from high-throughput sequencing reads. EMBnet J 2011;17:10–2.
38. Kim D, Langmead B, Salzberg SL. HISAT: a fast spliced aligner with low memory requirements. Nat Methods 2015;12:357–60.
39. Anders S, Pyl PT, Huber W. HTSeq–a Python framework to work with high-throughput sequencing data. Bioinformatics 2015;31:166–9.
40. McCarthy DJ, Chen Y, Smyth GK. Differential expression analysis of multifactor RNA-Seq experiments with respect to biological variation. Nucleic Acids Res 2012;40:4288–97.
41. Masoodi KZ, Xu Y, Dar JA, Eisermann K, Pascal LE, Parrinello E, et al. Inhibition of androgen receptor nuclear localization and castration-resistant prostate tumor growth by pyrroloimidazole-based small molecules. Mol Cancer Ther 2017;16:2120–9.
42. Nelson PS, Clegg N, Arnold H, Ferguson C, Bonham M, White J, et al. The program of androgen-responsive genes in neoplastic prostate epithelium. Proc Natl Acad Sci U S A 2002;99:11890–5.
43. Hu R, Lu C, Mostaghel EA, Yegnasubramanian S, Gurel M, Tannahill C, et al. Distinct transcriptional programs mediated by the ligand-dependent full-length androgen receptor and its splice variants in castration-resistant prostate cancer. Cancer Res 2012;72:3457–62.
44. Sun S, Sprenger CC, Vessella RL, Haugk K, Soriano K, Mostaghel EA, et al. Castration resistance in human prostate cancer is conferred by a frequently occurring androgen receptor splice variant. J Clin Invest 2010;120:2715–30.
45. Li Y, Chan SC, Brand LJ, Hwang TH, Silverstein KA, Dehm SM. Androgen receptor splice variants mediate enzalutamide resistance in castration-resistant prostate cancer cell lines. Cancer Res 2013;73:483–9.
46. Hall JM, McDonnell DP. The estrogen receptor beta-isoform (ERbeta) of the human estrogen receptor modulates ERalpha transcriptional activity and is a key regulator of the cellular response to estrogens and antiestrogens. Endocrinology 1999;140:5566–78.
47. Mukherjee A, Kirkovsky L, Yao XT, Yates RC, Miller DD, Dalton JT. Enantioselective binding of Casodex to the androgen receptor. Xenobiotica 1996;26:117–22.
48. Cockshott ID. Bicalutamide: clinical pharmacokinetics and metabolism. Clin Pharmacokinet 2004;43:855–78.
49. Sramkoski RM, Pretlow TG II, Giaconia JM, Pretlow TP, Schwartz S, Sy MS, et al. A new human prostate carcinoma cell line, 22Rv1. In Vitro Cell Dev Biol Anim 1999;35:403–9.
50. Dehm SM, Schmidt LJ, Heemers HV, Vessella RL, Tindall DJ. Splicing of a novel androgen receptor exon generates a constitutively active androgen receptor that mediates prostate cancer therapy resistance. Cancer Res 2008;68:5469–77.
51. Yu Z, Chen S, Sowalsky AG, Voznesensky OS, Mostaghel EA, Nelson PS, et al. Rapid induction of androgen receptor splice variants by androgen deprivation in prostate cancer. Clin Cancer Res 2014;20:1590–600.
52. Hu R, Dunn TA, Wei S, Isharwal S, Veltri RW, Humphreys E, et al. Ligand-independent androgen receptor variants derived from splicing of cryptic exons signify hormone-refractory prostate cancer. Cancer Res 2009;69:16–22.
53. Tepper CG, Boucher DL, Ryan PE, Ma AH, Xia L, Lee LF, et al. Characterization of a novel androgen receptor mutation in a relapsed CWR22 prostate cancer xenograft and cell line. Cancer Res 2002;62:6606–14.
54. Yu Z, Cai C, Gao S, Simon NI, Shen HC, Balk SP. Galeterone prevents androgen receptor binding to chromatin and enhances degradation of mutant androgen receptor. Clin Cancer Res 2014;20:4075–85.

55. Li Y, Hwang TH, Oseth LA, Hauge A, Vessella RL, Schmechel SC, et al. AR intragenic deletions linked to androgen receptor splice variant expression and activity in models of prostate cancer progression. Oncogene 2012;31:4759–67.
56. Li Y, Alsagabi M, Fan D, Bova GS, Tewfik AH, Dehm SM. Intragenic rearrangement and altered RNA splicing of the androgen receptor in a cell-based model of prostate cancer progression. Cancer Res 2011;71:2108–17.
57. Liu C, Lou W, Zhu Y, Yang JC, Nadiminty N, Gaikwad NW, et al. Intracrine androgens and AKR1C3 activation confer resistance to enzalutamide in prostate cancer. Cancer Res 2015;75:1413–22.
58. Nadiminty N, Tummala R, Liu C, Yang J, Lou W, Evans CP, et al. NF-B2/p52 induces resistance to enzalutamide in prostate cancer: role of androgen receptor and its variants. Mol Cancer Ther 2013;12:1629–37.